

## SETUP OF A HIGH-SPEED OPTICAL SYSTEM FOR THE CHARACTERIZATION OF CAVITATION INSTABILITIES IN SPACE ROCKET TURBOPUMPS

**Angelo Cervone/ ALTA S.p.A.**  
Project Manager  
[a.cervone@alta-space.com](mailto:a.cervone@alta-space.com)

**Lucio Torre/ ALTA S.p.A.**  
Research Engineer  
[l.torre@alta-space.com](mailto:l.torre@alta-space.com)

**Domenico Fotino/ University of Pisa**  
MS student  
[domenico.fotino@tiscalinet.it](mailto:domenico.fotino@tiscalinet.it)

**Cristina Bramanti/ ESA-ESTEC**  
Post-Doc Fellow  
[Cristina.Bramanti@esa.int](mailto:Cristina.Bramanti@esa.int)

**Luca d'Agostino/ University of Pisa**  
Professor  
[luca.dagostino@ing.unipi.it](mailto:luca.dagostino@ing.unipi.it)

### ABSTRACT

The present paper illustrates the set-up and the preliminary results of an experimental investigation of cavitation flow instabilities carried out by means of a high-speed camera on a three bladed inducer in the CPRTF (Cavitating Pump Rotordynamic Test Facility) at Alta S.p.A. The brightness thresholding technique adopted for cavitation recognition is described and implemented in a semi-automatic algorithm. In order to test the capabilities of the algorithm, the mean frontal cavitating area has been computed under different operating conditions. The tip cavity length has also been evaluated as a function of time. Inlet pressure signal and video acquisitions have been synchronized in order to analyze possible cavitation fluid-dynamic instabilities both optically and by means of pressure fluctuation analysis. Fourier analysis showed the occurrence of a cavity length oscillation at a frequency of 14.7 Hz, which corresponds to the frequency of the rotating stall instability detected by means of pressure oscillation analysis.

### NOMENCLATURE

$A$	= amplitude of oscillations
$b_t$	= blade thickness
$d$	= $\frac{b_t}{n}$
$f$	= frequency
$n$	= normal blade spacing
$p_{in}$	= inlet pressure
$p_v$	= vapor pressure
$Q$	= volumetric flow rate
$r_T$	= inducer blade tip radius
$S_{cav}$	= total cavitating surface on each blade
$S_{flow}$	= inducer frontal surface
$t$	= time
$\alpha$	= incidence angle

$\beta_b$	= blade angle
$\Omega$	= rotational speed
$\Phi$	= flow coefficient $\Phi = \frac{Q}{\pi\Omega r_T^3}$
$\phi$	= phase of oscillations
$\rho$	= density
$\sigma$	= cavitation number
$\sigma_c$	= choked cavitation number
$\theta$	= azimuthal coordinate
$\Delta\theta$	= azimuthal extension of the cavity at the tip of the blades

### INTRODUCTION

In space propulsion, propellant feed turbopumps are a crucial component of all primary propulsion concepts powered by liquid propellant rocket engines. Severe limitations are associated with the design of high power density, dynamically stable machines capable of meeting the extremely demanding suction, pumping and reliability requirements of current space transportation systems (Stripling & Acosta, 1962).

In most cases these pumps employ an inducer upstream of the centrifugal stage(s) in order to improve the suction performance and reduce the propellant tank pressure and weight. Significant cavitation levels typically occur in inducers and often lead to the development of flow instabilities that can seriously degrade the performance of the machine, or even cause its rapid failure.

According to Brennen (1994), these flow instabilities can be divided in three main categories: global oscillations, local oscillations and instabilities caused by radial or rotordynamic forces. Some of the most interesting and well-recognized instabilities in pumps and axial inducers are global oscillations, such as the *rotating stall* and the *rotating cavitation*, propagating in the azimuthal direction at angular speeds different from that

of the pump (typically subsynchronous for rotating stall and supersynchronous for rotating cavitation). Other global oscillations are the *surge* and the *cavitation auto-oscillations*, system instabilities involving strong longitudinal flow and pressure oscillations of the whole suction line, typically occurring in noncavitating pumps for positive slopes of the characteristic curve (surge) and near breakdown conditions in cavitating turbopumps (cavitation auto-oscillations).

Experimental investigations on the instabilities triggered by cavitation in axial inducers have been recently carried out at Alta S.p.A. (Cervone, Testa, Bramanti, Rapposelli and d'Agostino, 2005; Cervone, Torre, Bramanti, Rapposelli and d'Agostino, 2005). Experiments were conducted in the CPTF (Cavitating Pump Test Facility), specifically intended for general-purpose experimentation on cavitating/noncavitating turbopumps, and its upgraded version, the CPRTF (Cavitating Pump Rotordynamic Test Facility), which is especially dedicated to the investigation of rotordynamic fluid forces in forced vibration experiments with adjustable rotational and whirl speeds.

Tsujimoto and his collaborators (1997) introduced for the first time the cross-correlation and phase analysis technique in order to detect the frequency of oscillation and the spatial characteristics (i.e. rotating or axial) of the cavitating flow oscillations. This technique has also been used in Alta's experiments (Cervone *et al.*, 2005).

The characterization of the flow instabilities by means of unsteady pressure measurements, however, is significantly more effective if accompanied by optical visualization of the cavitating flow on the inducer blades by means of high-speed movies.

Using the combination of these techniques, Tsujimoto and his collaborators (1997) detected the occurrence of rotating cavitation and other modes of oscillation on a scaled model of the LE-7 LOX turbopump inducer. They concluded that the rotating cavitation was probably caused by the occurrence of five cavitation regions extending upstream from the tip of the blades and slowly rotating. By analysis of the high-speed movies they also detected a form of instability characterized by axial fluctuations (cavitation surge).

Kamijo and his collaborators (1994) detected the occurrence of a supersynchronous frequency in the spectra of the inlet pressure fluctuations and using high speed camera movies they could state that it was caused by the circumferential cavity length oscillation at same frequency. They observed that both the tip vortex cavitation and the blade surface cavitation oscillated at approximately the same supersynchronous frequency and the same phase.

Using a high speed camera at 7000 fps, Hashimoto *et al.* (1997) plotted the cavitating surface as a function of the number of inducer revolutions, on a three bladed inducer with dimensions similar to those of the LE-7 LOX pump inducer. They detected various modes of oscillation, including a backward-rotating and a forward-rotating cavitation, an attached cavitation and a low cycle oscillation.

Recently, in french research laboratories, Joussellin *et al.* (2001) used frontal images of a four-bladed inducer in order to extract the cavitating regions by means of an image processing code developed by the National Institute of Health. They plotted the non-dimensional cavitating area as a function of the cavitation number at constant flow rate and as a function of the flow rate at constant cavitation number.

This paper is aimed at illustrating the following aspects of the present research activity at Alta S.p.A.:

- set up of the optical system in order to record frontal high-speed movies (up to 16000 fps) on a three-bladed inducer;
- implementation of an image processing algorithm for extracting the blade cavitating areas from every frame;
- implementation of an automatic algorithm for calculating the tip cavity length;
- estimation and analysis of the blade cavitating areas;
- spectral analysis of the inlet pressure fluctuations by means of piezoelectric pressure transducers;
- spectral analysis of the cavity length fluctuations.

## EXPERIMENTAL APPARATUS

The Cavitating Pump Rotordynamic Test Facility (CPRTF, Figure 1) has been designed to experimentally characterize the performance of pumps in a wide variety of alternative configurations (axial, radial or mixed flow, with or without an inducer; Rapposelli, Cervone and d'Agostino, 2002). The facility operates in water at temperatures up to 90 °C and is intended as a flexible apparatus readily adaptable to conduct experimental investigations on virtually any kind of fluid dynamic phenomena relevant to high performance turbopumps.

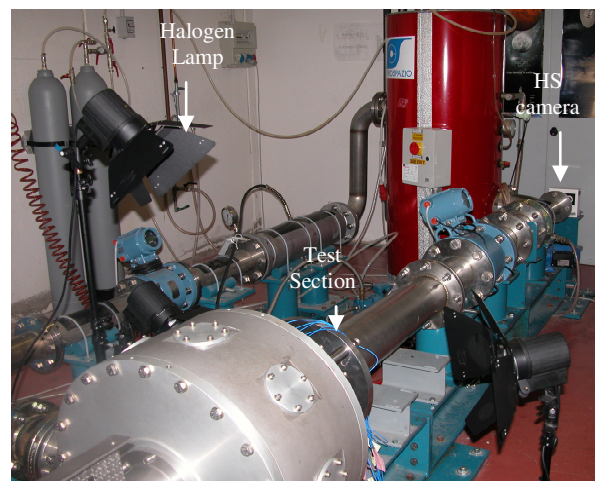


**Figure 1. The Cavitating Pump Rotordynamic Test Facility.**

The test section (Figure 2) is equipped with a rotating dynamometer, for the measurement of the forces and moments acting on the impeller, and a mechanism for adjusting and rotating the eccentricity of the impeller axis in the range  $0 \div 2$  mm and  $\pm 3000$  rpm. The inlet section,

made of Plexiglas, is transparent in order to allow for optical visualization of cavitation on the test inducer.

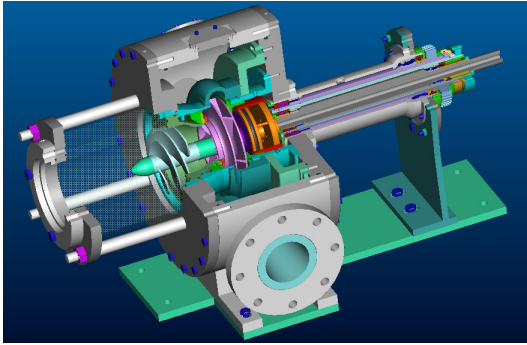


**Figure 2. Cut-out drawing of the CPRTF test section.**

The adjustable physical parameters of the experimental set-up include the pump rotating speed and acceleration (by means of the engine controls), the mass flow (by means of a lamination valve), the temperature and pressure of the working fluid (by means, respectively, of a heat exchanger and a bladder placed inside the tank).

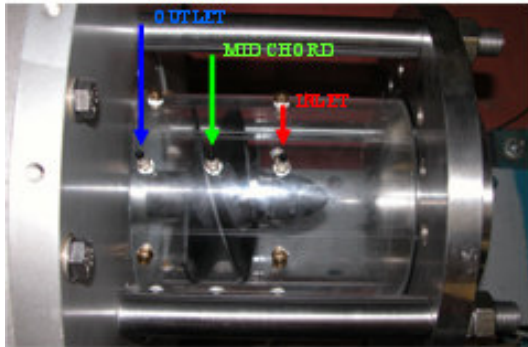


**Figure 3. The inlet section of the facility instrumented with piezoelectric pressure transducers.**

For the present experimental work the facility was assembled in a simplified configuration without the rotating dynamometer. The test section was equipped with three different series of pressure transducers. The inlet pressure is measured by means of an absolute pressure transducer installed upstream of the Plexiglas inlet section (Druck, model PMP 1400, 0÷1.5 bar operating range, 0.25% precision class). The pressure rise, necessary for the characterization of the pump performance, is measured by means of two redundant differential pressure transducers installed between the inlet and the outlet sections of the test pump (Kulite, model BMD 1P 1500 100, 0-100 psid operating range, 0.1% precision class; Druck, model PMP 4170, 0÷1 bar operating range, 0.08% precision class). The pressure fluctuations are analyzed by equipping the inlet section (Figure 3) with flush-mounted piezoelectric pressure transducers (PCB M112A22, ICP® voltage mode-type, 0.1% class) located at three axial stations (inducer inlet, outlet and at the middle of the axial chord of the blades, Figure 3). At each axial station at least two transducers have to be mounted with a given angular spacing, in order to cross-correlate their signals for coherence and phase analysis. As a result, waterfall plots of the power spectral

density of the pressure fluctuations can be obtained as functions of the cavitation number  $\sigma = (p_{in} - p_v) / \frac{1}{2} \rho \Omega^2 r_T^2$ , in order to detect the occurrence of instabilities. The axial or azimuthal nature of the detected instabilities (and, in the second case, the number of rotating cells involved) can be determined by means of cross-correlation of the pressure signals from different locations.

The capabilities of the test facility have been improved after the installation of an integrated system for the optical analysis of the cavitating flow. The core of the system is represented by a high-speed video camera, Fastec Imaging model Ranger having a record rate variable from 125 fps (max resolution 1280x1024) to 16000 fps (max resolution 1280x32). It uses a monochrome CMOS sensor and its recording mode can be manual or triggered by the connection with a Personal Computer by means of USB port. The shutter speed ranges from 1x to 20x the recording rate. The required illumination level is provided by three halogen lamps produced by Hedler, each one having a power of 1250 W. The camera can also be synchronized with a stroboscopic light, Drelloscop 3009, having a maximum flash frequency of 1000 lamps/second with a frequency accuracy of 0.001%. The optical system is completed by a Nikon Coolpix 5700 digital photo camera, with optical 8x zoom, digital 4x zoom, a focal distance from 8.9 to 71.2 millimeters and a shutter speed from 1/4000 sec to 8 sec.

The characteristics of the facility make it possible to record both side movies, through the Plexiglas inlet section, and frontal movies, through an optical access placed at the end of the suction line (Figure 4). Side movies provide indications on the extension of cavitation in the blade channels, whereas the frontal ones give information about the radial and circumferential extension of the cavities on the blades.

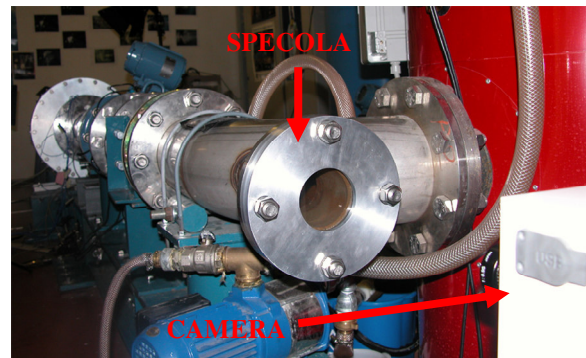


**Figure 4. The optical access at the end of the facility suction line.**

The preliminary results illustrated in this paper refer to the FIP162 inducer (Figure 5): it is a 3-bladed, aluminum-made axial pump of extremely simple helical geometry, with a tip radius of 81 mm, a hub radius of 22.5 mm, a tip blade angle of 9°, a tip solidity of 3.05 and 2 mm thick back-swept blades with blunt leading and trailing edges. It is manufactured by Fabbrica Italiana Pompe (FIP) S.p.A. for the food industry by welding the

blades on the hub, therefore it does not satisfy stringent geometric tolerances.



Figure 5. The FIP162 inducer.

### IMAGE PROCESSING ALGORITHM

A semi-automatic image processing algorithm has been developed to extract the regions of the image where cavitation is present. This algorithm has been implemented in a code that allows for automatically processing the frames of the movies taken by the high-speed camera and for analyzing the movie using the processed frames. The algorithm has been implemented in *Matlab*<sup>®</sup> and its flow chart is shown in Figure 6. The input is a frame in gray-scale format: a typical input image is shown in Figure 7 (left).

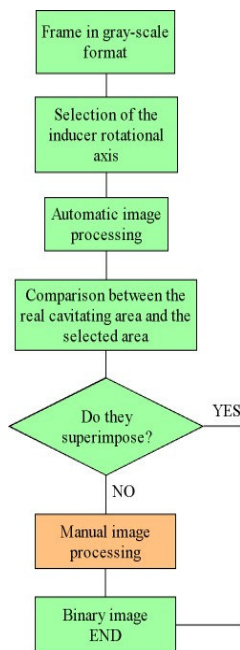


Figure 6. Flow chart of the semi-automatic algorithm.

The first step of the procedure is the manual selection of the inducer rotational axis for the first frame of the movie; this operation allows to rotate all the processed frames around this point in order to obtain a movie in which the position of the blades is fixed.

The next step is the so-called “segmentation technique” by which the cavitating regions are separated by the rest of the image. Several segmentation techniques have been proposed in the past by the open literature (see for example Gonzales, 2002): the thresholding technique has been the one used in the present activity. By this technique, the original grayscale image is converted in a binary image: the pixels having an intensity in the original image greater than a certain threshold value are set equal to 1 (i.e., they become white pixels), while all other pixels are set equal to 0 (i.e., they become black pixels). Despite its implementation simplicity, the main problem of this technique is the evaluation of the right value to be attributed to the threshold. There are several methods to automatically find this value according to the image histogram properties (Gonzalez 2002, Kato *et al.* 2003, Otsu 1979). The simplest way to find the right threshold is to choose an intermediate value between the two peaks shown by the typical brightness histogram of the input frame (Figure 8).

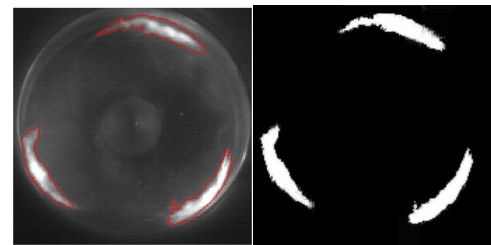


Figure 7. Comparison between the original frame (left) and the processed binary image (right) in a sample case.

In the present case it has not been possible to find a threshold value for the frame as a whole, so different threshold values have been used for the different regions in the image: the input frame is divided in several circular sectors (Figure 9) and an automatic threshold value, evaluated using the Otsu’s method (Otsu, 1979), is given for each sector.

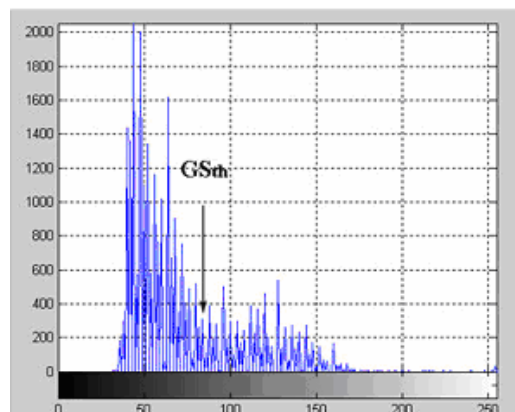
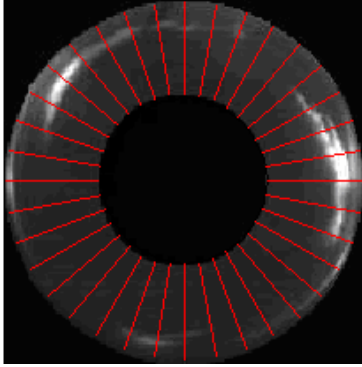


Figure 8. Typical brightness histogram of an input frame.

An analysis of the brightness histogram for each circular sector (Figure 10) showed that the standard deviation for the sectors in which there is no cavitation is

very low, so the pixels of these sectors are set equal to 0 without setting any threshold value. Besides, in order to better analyze the cavitating regions on the blades, the central portion of the image (where other cavitating phenomena often occur) and the region outside the inducer are covered with black pixels (masked portions in Figure 9). So, by calibrating the angular division of the frame, a good first-tentative image segmentation is obtained.



**Figure 9.** Example of the image division and the masked portions.

The contour of the white regions in the first-tentative binarized image is then superimposed to the gray-scale frame (red contour in Figure 7, left): if it does not superimpose to the effective cavitating regions, the operator can manually process the frame selecting the right cavitating areas and setting a new threshold value by a trial-and-error technique until the right value is found (i.e. the value that produces a good result as by the operator's judgement [Gonzalez 2002]). An example of the resulting binary image is shown in Figure 7 (right).

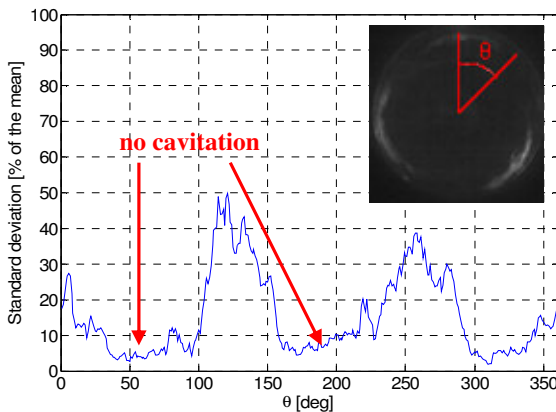


**Figure 10.** Standard deviation of the brightness histogram as a function of the azimuthal coordinate  $\theta$ .

### BLADE CAVITATING AREA ESTIMATION

The total frontal area of the cavitating regions on the inducer blades ( $S_{cav}$ ) has been estimated by mediating the number of white pixels in all the frames of a movie taken at given flow conditions. This value has been normalized using the total frontal area of the inducer ( $S_{flow}$ ).

A standard procedure has been adopted for the tests. The working fluid has been deaerated before every test.

In order to improve the image quality, excessively high cavitation levels have not been reached during the tests. For this reason, the inducer rotational speed has been set equal to 1500 rpm. Nevertheless, at low flow coefficients and cavitation numbers, the image processing algorithm described in the previous Section can not be used properly, due to the significant number of vortices and large cavitation regions in the inducer inlet flow. The water quality is significantly degraded, with a large number of cavitating nuclei and consequently adverse effects on light diffusion (Figure 11).

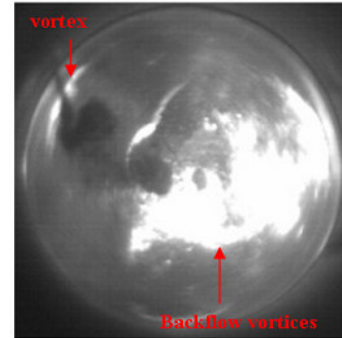


**Figure 11.** Example of a frame which can not be analyzed using the image processing.

High speed movies have been recorded at constant flow rate, while the inducer inlet pressure has been decreased from high to low values using the vacuum pump.

The camera frame rate has been set equal to 1000 fps (i.e. 40 frames/revolution at 1500 rpm), at an image resolution of 640x480 pixels. This setup gave the possibility of optically analyzing the cavitation instabilities detected on the same inducer by unsteady pressure measurement analysis.

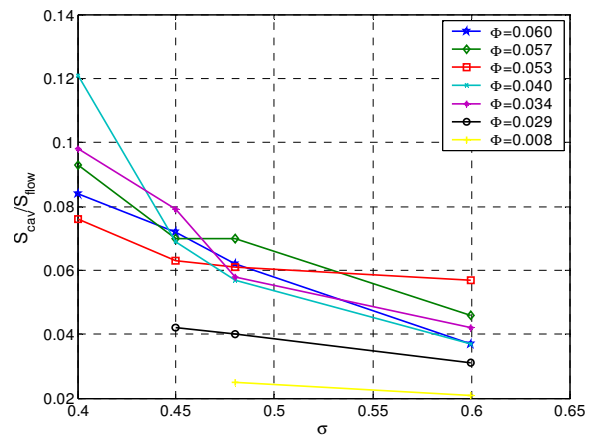


**Figure 12.** Frontal cavitating surface as a function of the cavitation number for several values of the flow coefficient.

The plot presented in Figure 12 shows the normalized frontal cavitating surface as a function of the cavitation number for several values of the flow coefficient. It is evident that the cavitating surface tends to decrease when the cavitation number increases. This aspect is also

evident by observation of the frames shown in Figure 13 and referred to a particular value of the flow coefficient.

The plot presented in Figure 14, on the other hand, shows the normalized frontal cavitating surface as a function of the flow coefficient for several values of the cavitation number. It can be observed that the cavitating surface tends to decrease when the flow coefficient decreases.

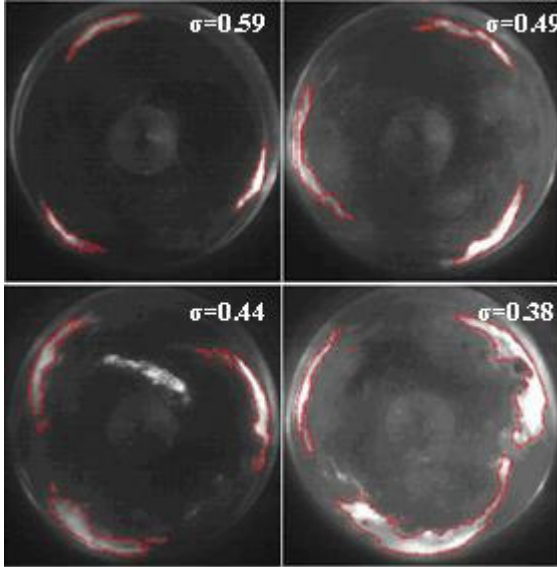


**Figure 13. Cavitating area development for a particular flow condition. ( $\Phi = 0.04$ ,  $\Omega = 1500$  rpm, frame sample rate = 1000 fps).**

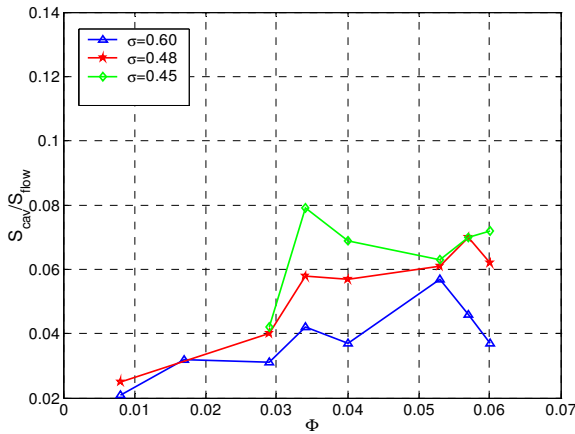


**Figure 14. Frontal cavitating surface as a function of the flow coefficient for several values of the cavitation number.**

The trend shown in Figure 14 is in agreement with the free streamline solution proposed by Brennen and Acosta (1973). Their analytical model gives the following equation for the choked cavitation number (defined as the minimum cavitation number at which the cavity becomes infinitely long and below which there are no solutions):

$$\sigma_c = \left[ 1 + \sin\left(\frac{\alpha}{2}\right) \sec\left(\frac{\beta_b}{2}\right) \sin\left(\frac{\beta_b - \alpha}{2}\right) + 2d \sin^2\left(\frac{\beta_b}{2}\right) \right]^2 - 1$$

Figure 15 shows the choked cavitation number for the FIP162 inducer, as a function of the flow coefficient, according to the Brennen-Acosta model. It increases with the flow coefficient and it reaches a maximum for  $\Phi = 0.08$ . This results is in agreement with the experimental observations presented in Figure 14.

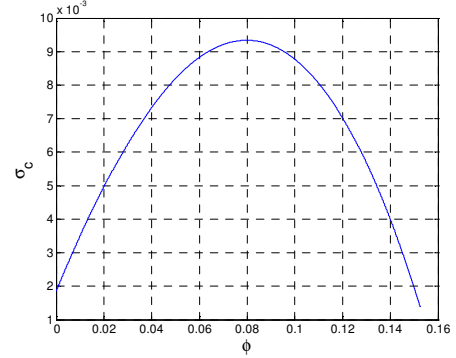


**Figure 15. Choked cavitation number, as a function of the flow coefficient, for the FIP162 inducer.**

### TIP CAVITY LENGTH ESTIMATION

The tip cavity length has been estimated using an automatic algorithm which scans every binary frame with a line rotating around the inducer axis at an angular pitch of  $1^\circ$ . When a white pixel is found along the scanning line after a completely black line, the cavitating region is assumed to begin; on the other hand, when every pixel along the scanning line becomes black, the cavitating region is assumed to finish (Figure 16). The length of the cavitating region is finally estimated by multiplying its azimuthal extension ( $\Delta\theta$ ) by the radius at which the cavitating region has been examined.

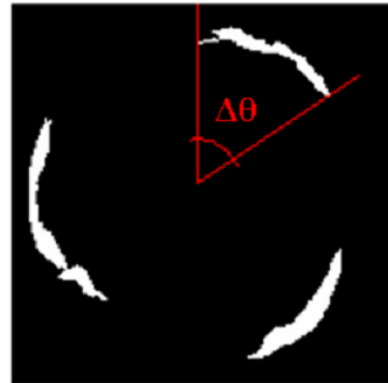


**Figure 16. Evaluation of the azimuthal extension of the cavitation on a blade.**

Sometimes the cavitating region appears to be fragmented. This is due to the separation of small cavitating areas and to the presence of vortices between the real blade surface and the camera lens (Figure 11). In this case the algorithm takes into account the angular separation between the different cavitating regions and, if they are sufficiently close, they are considered as an unique cavitating region. Otherwise, if the cavitating regions are sufficiently distant, they are considered as

effectively separated and only the length of the first one is taken into account.

This procedure has been applied to a binarized movie whose frames have been rotated around the inducer rotational axis in order to obtain fixed blade position. The following plots (Figure 17) show the length of the cavitating region on the blades as a function of time, at given flow conditions.

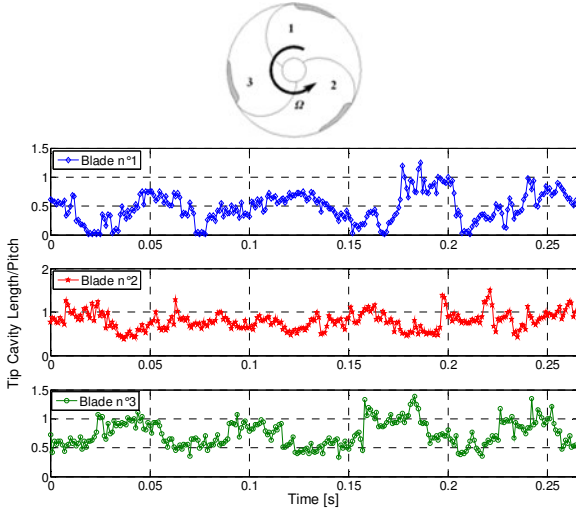


**Figure 17. Length of the cavitating regions on the blades as a function of time ( $\Phi = 0.034$ ,  $\sigma = 0.52$ ,  $\Omega = 1500$  rpm, frame sample rate = 1000 fps).**

#### FOURIER ANALYSIS OF THE INLET PRESSURE AND CAVITY LENGTH FLUCTUATIONS

In the experiments for the characterization of the flow instabilities six piezoelectric transducers were mounted at the inducer inlet station (Figure 3) at an angular spacing of  $45^\circ$  (Figure 18), in order to characterize the occurrence and nature of instabilities.

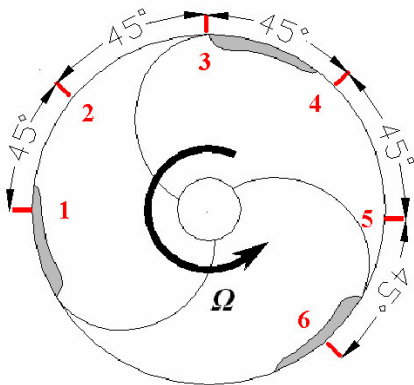


**Figure 18. Schematic of the piezoelectric transducers position at the inlet station.**

Examination of the waterfall plots obtained in a previous paper (Cervone *et al.*, 2005) shows the occurrence of several forms of instabilities. Among these, the rotating stall has been analyzed by means of both the inlet pressure fluctuations and the tip cavity length oscillations. To this purpose, pressure and movie acquisitions have been synchronized and different flow

conditions have been investigated based on the results of the previous analysis (Cervone *et al.*, 2005).

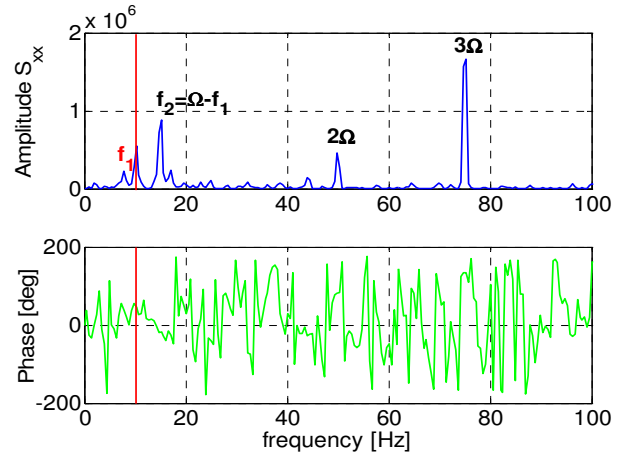


**Figure 19. Power density spectrum and phase of the cross-correlation of the pressure signals of two transducers with  $45^\circ$  angular separation ( $\Phi=0.034$ ,  $\sigma=0.52$ ,  $\Omega=1500$  rpm).**

Figure 19 shows the power density spectrum and the phase of the cross-correlation of the pressure signals by two transducers with  $45^\circ$  angular separation, calculated at a flow condition for which the rotating stall ( $f_i$  frequency) is well recognizable. It can be observed that the phases of the cross-correlation are approximately equal to the adopted transducer angular spacing (Table 1). For this reason,  $f_i$  represents a one cell sub-synchronous rotating phenomenon ( $0.41\Omega$ ). The spectrum also shows a well-defined frequency peak at  $f_2=\Omega-f_i$ , probably caused by a non linear interaction between the rotating stall and the inducer rotational frequency, which suggests that  $f_i$  represents a forward-rotating phenomenon.

<b>frequency</b>	$f_1=10.3$ Hz
<b>Phase 1-2</b>	$45^\circ$
<b>Phase 1-3</b>	$83^\circ$
<b>Phase 1-4</b>	$126^\circ$
<b>Phase 1-5</b>	$175^\circ$
<b>Phase 1-6</b>	$220^\circ$

**Table 1. Phase of the cross-correlation between the signal obtained by transducer 1 and the other transducers shown in Figure 18.**

Fourier analysis of the tip cavity length oscillations shown in Figure 17, calculated at the same flow conditions of Figure 19, gives the results presented in Figure 20.

A well defined peak is detected in the power spectrum at a frequency of 14.7 Hz ( $f_c$ ). The cross-correlation phases are  $120^\circ$  (blade 3-blade 2),  $155^\circ$  (blade 2-blade 1) and  $85^\circ$  (blade 1-blade 3). This means that the phenomenon is rotating clockwise in the rotating coordinate frame. The ratio of the mean angular

separation of two adjacent cavitating regions to the relative cross-correlation phase is about one and this means that the oscillation involves just one single rotating cell.

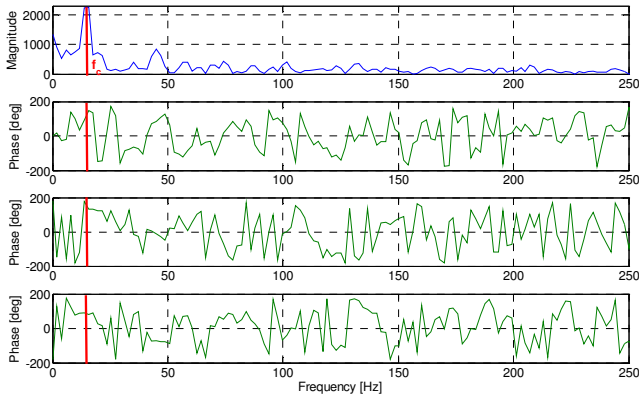


**Figure 20. Power spectrum of the tip cavity length on third blade (blue). Phase of the cross-correlation between 3<sup>rd</sup> and 2<sup>nd</sup> blade (second plot), 2<sup>nd</sup> and 1<sup>st</sup> blade (third plot), 1<sup>st</sup> and 3<sup>rd</sup> blade (fourth plot).**

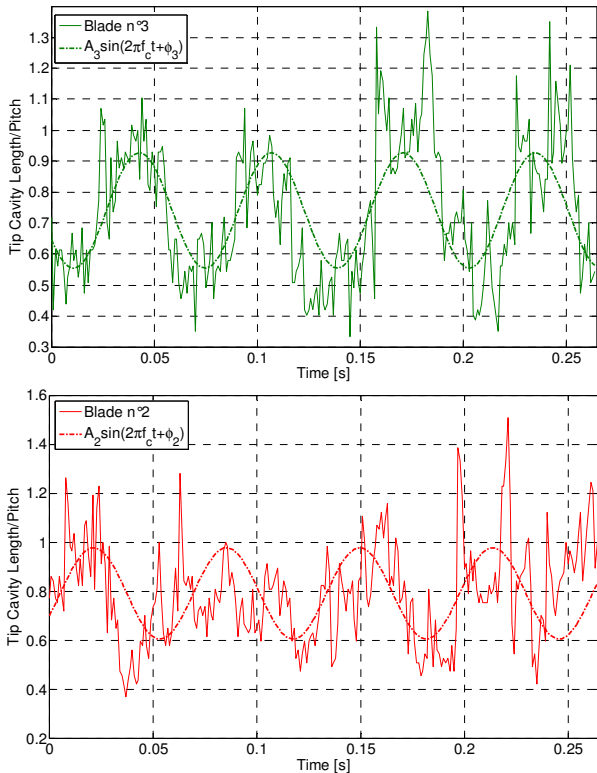


**Figure 21. Sinusoidal signal at frequency  $f_c$  superimposed to the measured non-dimensional tip cavity length for blade 3 (top) and blade 2 (bottom).**

The detected rotating stall has a frequency of  $0.41\Omega$  in a fixed coordinate frame. As a consequence, in a coordinate frame rotating with the blades (as the one used to estimate the cavity length) this frequency becomes 14.7 Hz, which is just the observed value of  $f_c$ .

Figure 21 (top) shows a sinusoidal signal at frequency  $f_c$ , whose magnitude and phase have been calculated

using a trial-and-error technique, superimposed to the non-dimensional tip cavity length on the third blade, while Figure 21 (bottom) shows the same sinusoidal signal shifted of an angle equal to the phase of the cross-correlation between blade 3 and blade 2.

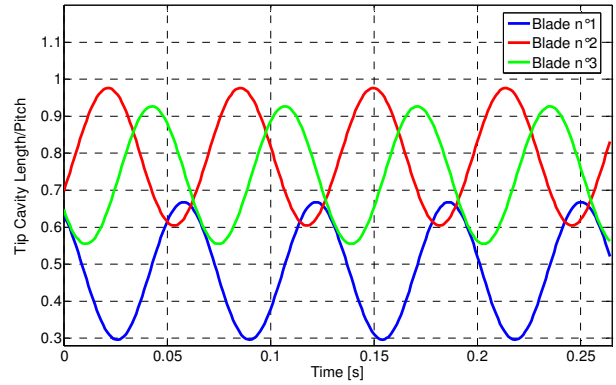


**Figure 22. Oscillation of the cavity length on the blades of the FIP inducer.**

Figure 22 shows the sinusoidal signals of Figure 21 together with that obtained for the remaining blade (same frequency, phase calculated from the cross-correlation analysis). It is evident that the cavity propagates clockwise from the first blade to the third blade. It can also be observed that the mean cavity length on the first blade is lower than the other two (asymmetric cavitation, Figure 23).

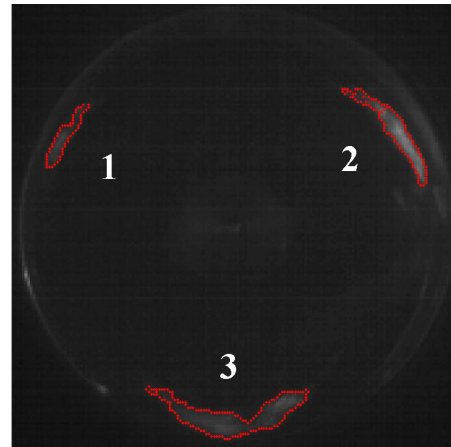


**Figure 23. Example of asymmetric blade cavitation.**

## CONCLUSIONS

The present research activity has allowed for the development and successful validation of a viable and effective tool, based on optical processing of high-speed video movies for quantitative analysis and diagnostics of cavitation instabilities in turbopump inducers. The capabilities of the semi-automatic algorithm created to implement the proposed technique have been improved by developing a procedure for the estimation of the frontal cavitating surface and the extension of the cavitating regions on the blades.

The application of the above technique to the analysis of cavitation in a test inducer lead to the detection of the

same rotating stall instability observed under the same operating conditions by means of Fourier analysis of the inlet pressure signals. The results confirm the potential of the proposed method in the characterization of cavitation-induced instabilities and suggest the possibility of extracting additional useful information on the nature, extent and location of the cavitating regions on the inducer blades.

## ACKNOWLEDGMENTS

The present activity has been funded by the Agenzia Spaziale Italiana under contract No. I/016/05/0 for fundamental research, whose support is gratefully acknowledged. The authors would like to express their gratitude to Profs. Mariano Andrenucci, Renzo Lazzeretti and Fabrizio Paganucci of the Dipartimento di Ingegneria Aerospaziale, Università di Pisa, Pisa, Italy, for their constant and friendly encouragement.

## REFERENCES

- Stripling L.B. and Acosta A.J. "Cavitation in Turbopumps – Part 1", ASME J. Basic Eng., Vol. 84, pp. 326-338, 1962.
- Brennen C.E., "Hydrodynamics of Pumps", Concepts ETI, Inc. and Oxford University Press, 1994.
- Cervone A., Torre L., Fotino D., d'Agostino L., Bramanti C., "Characterization of Cavitation Instabilities in Axial Inducers by Means of High-Speed Movies", 42nd AIAA/ASME/SAE/ASEE Joint Propulsion Conference, Sacramento, California, USA, 2006.
- Cervone A., Testa R., Bramanti C., Rapposelli E. and d'Agostino L., "Thermal Effects on Cavitation Instabilities in Helical Inducers", AIAA Journal of Propulsion and Power, Vol. 21, No. 5, Sep-Oct 2005, pp. 893-899.
- Cervone A., Torre L., Bramanti C., Rapposelli E. and d'Agostino L., "Experimental Characterization of the Cavitation Instabilities on the Avio FAST2 Inducer", 41th AIAA/ASME/SAE/ASEE Joint Propulsion Conference, Tucson, Arizona, USA, 2005.
- Tsujimoto Y., Yoshida Y., Maekawa Y., Watanabe S., Hashimoto T., "Observation of Oscillating Cavitation of an Inducers", ASME J. Fluids Eng. ing, Vol. 119, pp. 775-781, 1997.
- K. Kamijo, T. Shimura, Y. Tsujimoto, "Experimental and Analytical Study of Rotating Cavitation", Cavitation and gas liquid flow in fluid machinery and devices, ASME 1994.
- Hashimoto T., Yoshida M., Watanabe M., Kamijo K., Tsujimoto Y., "Experimental Study of Rotating Cavitation of Rocket Propellant Pump Inducers", J. Propulsion and Power, Vol. 13, N. 4., pp. 488-494, 1997.
- Jousselin F., Courtot Y., Coutier-Delgosha O., Reboud J.L., "Cavitating inducer instabilities : experimental analysis and 2D numerical simulation of unsteady flow in blade cascade", CAV2001, 2001.
- Rapposelli E., Cervone A. & d'Agostino L., "A New Cavitating Pump Rotordynamic Test Facility", AIAA Paper 2002-4285, 38th AIAA/ASME/SAE/ASEE Joint

Propulsion Conference, Indianapolis, IN, USA, July 8-11, 2002.

Gonzalez R.C., Woods R.E., "Digital Image Processing", Prentice-Hall, 2002.

Kato K., Matudaira Y. and Obara H., "Flow Visualization of Cavitation with Particle and Bubble Image Processing", ASME FEDSM summer meeting, Honolulu, Hawaii, USA, 2003.

Otsu N., "A Threshold Selection Method from Gray-Level Histograms", IEEE Transactions on Systems, Man and Cybernetics, vol. 9, no. 1, pp. 62-66, 1979.

Brennen C.E., Acosta A.J., "Theoretical, quasistatic analyses of cavitation compliance in turbopumps", Journal of Spacecraft and Rockets, 10, No. 3, 175-180, 1973.